





## Paper

# Global stabilization for nonlinear two-port characteristics of bidirectional DC/DC converter and its application to peer-to-peer energy transfer

Kenta Yamamoto <sup>1</sup>, Takashi Hisakado <sup>1</sup>,  
Mahfuzul Islam <sup>1</sup>, and Osami Wada <sup>1</sup>

<sup>1</sup> Department of Electrical Engineering, Kyoto University  
Kyotodaigakukatsura, Nishikyo-ku, Kyoto 615-8510, Japan

Received October 10, 2022; Revised December 23, 2022; Published April 1, 2023

**Abstract:** A global stabilization method for the conversion characteristics of a bidirectional DC/DC converter and its application in peer-to-peer energy transfer systems is described. Peer-to-peer energy transfer is a control strategy in which the supply and load cooperate to transmit power, and it requires the global operation of the converter. According to the power relation, the bidirectional DC/DC converter has two equilibrium points. To realize global stability, a unique equilibrium point is achieved by eliminating the untargated equilibrium point using the power relationship between the ports. Global stability is realized by setting feedback gains to converge globally to this equilibrium point. The experimental results demonstrate the global stability of the proposed method when applied to a stand-alone system and a peer-to-peer energy transfer system.

**Key Words:** bidirectional DC/DC converter, global stabilization, time-variable transformer, nonlinear two-port characteristics, peer-to-peer energy transfer

## 1. Introduction

The development of power electronics has facilitated flexible power conversion and control. In recent years, research and development of smart grids, renewable energy, and energy harvesting have progressed; therefore, the bidirectionality and flexibility of power conversion are required. In these systems, energy control is achieved by using two-port circuits to convert power. The modeling methods of power electronic circuits as two-port behavioral models have been studied for approximately half a century [1–3]. The two-port characteristics of the DC/DC converter driven by pulse width modulation (PWM) are modeled as an ideal linear transformer with a duty ratio transformation ratio [1, 2]. Because the duty ratio of PWM is a time variable, this circuit works as a time-variable transformer (TVT) [4]. The TVT is a lossless time-variable two-port circuit that can control two-port



characteristics by feedback operating points to the duty ratio [1, 5]. Research has been conducted on the realization of various two-port characteristics, such as gyrator [6], loss-free resistor [1], and lossless AC network elements [3].

The TVT can configure any two-port characteristics within the lossless and duty ratio constraints. In linear two-port circuits, the operating points between the ports correspond uniquely. However, the equilibrium is not uniquely determined owing to the energy relationships in the TVT. An example of this phenomenon is shown in Fig. 1(a). When we set the secondary-side operating point  $(v_2, i_2)$ , the primary-side operating points  $(v_1, i_1)$  are limited to a constant power line (red line) because of the power relationship between the ports. Two equilibrium points occur by two intersections of the constant power line and the  $i$ - $v$  characteristics of the power supply (blue line) connected to the primary-side port. These phenomena are similar to the two intersections in the constant-power load (CPL) shown in Fig. 1(b) [7–9]. Therefore, the two equilibrium points in the lossless two-port circuits are caused by the nonlinearity of the power. We refer to these phenomena as nonlinear two-port characteristics.

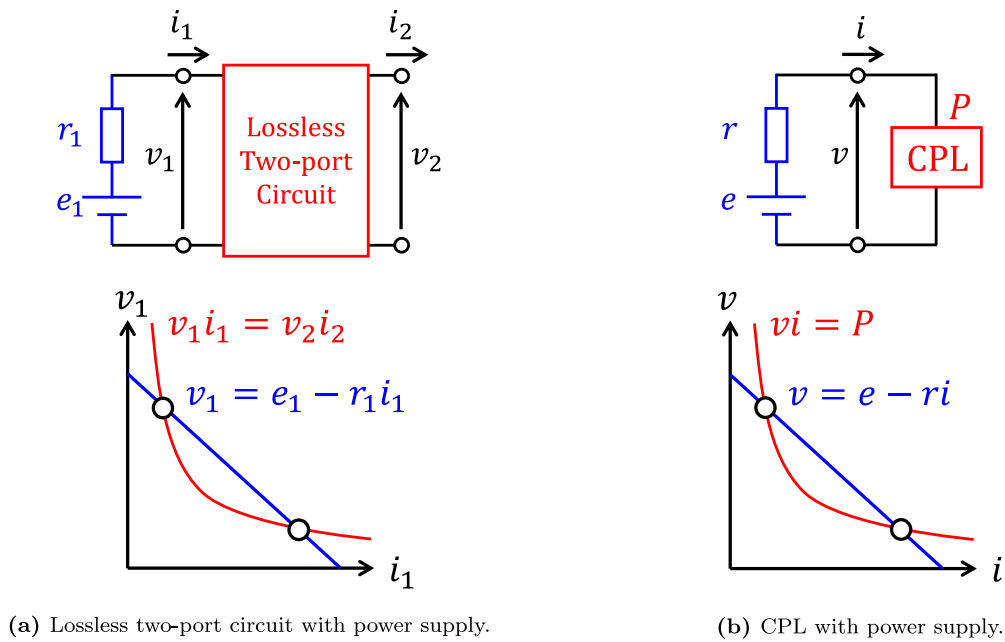


**Fig. 1.** Two equilibrium points of lossless two-port circuit and CPL.

These two operating points in the two-port circuits are observed using the global output characteristics of the power source. They feature the large-signal response of PV systems [10], stability analyses of battery charging, and stand-alone PV systems [11, 12]. When one equilibrium point is stabilized by feedback, the other point becomes unstable [10]. Multiple equilibrium points have also been reported in microgrid systems [13]. However, although there have been some individual discussions on the converter’s nonlinearity with an equilibrium point, there has not been an active discussion on the two-port characteristics. Because the converter is a two-port network element, it is critical to discuss these two equilibrium points from the perspective of its two-port characteristics. We formulate the power nonlinearities as nonlinear two-port characteristics of the converter and discuss their stability. We aim to achieve the global stabilization of these nonlinear two-port characteristics.

A unique equilibrium point and regions of attraction encompassing the operable region are necessary for the global stabilization of the nonlinear system. A typical approach is to perform exact linearization [14] on a nonlinear system. Exact linearization results in a unique equilibrium point, and global stability can be achieved by controlling the region of attraction to be the entire surface. Some studies applied exact linearization to boost converters [15], parallel buck converters [16] and microgrids [17]. Global stability can also be achieved using passivity-based control [18]. Passivity-based control achieves global stabilization of the system by rendering the control target passive. A

study has been conducted on applying passivity-based control to the constant power control of back converters to achieve global stability [19]. Thus, to achieve global stabilization of a nonlinear system, the equilibrium point must be made unique by feedback and its regions of attraction must be set all over the area. We achieve global stabilization by selecting an equilibrium point based on the power relationship at the converter and appropriately setting the regions of attraction.

We applied the proposed global stabilization method to a peer-to-peer energy transfer system. Peer-to-peer energy transfer is a control strategy in which the power supplies and loads cooperate to transmit energy [20]. In a converter network, the members of the network are coupled using a common bus. Peer-to-peer energy transfer achieves decoupling from other network members by matching changes in the order of milliseconds in the source and supply. This ensures that the bus voltage remains constant, regardless of the energy flow. Global stability is critical in peer-to-peer energy transfer because the operating point of the converter changes significantly during the transient process. We achieved a unique equilibrium point in the entire peer-to-peer energy transfer system using the proposed feedback, and global stabilization was realized by setting the feedback gains to converge globally to that equilibrium point.

The remainder of this paper is organized as follows. In Section 2, we define the nonlinear two-port characteristics of the bidirectional DC/DC converter. In Section 3, we describe the creation of a unique equilibrium point. In Section 4, we propose a gain that achieves global stabilization and applies the proposed method to a stand-alone converter. In Section 5, we apply the proposed method to stabilize a peer-to-peer energy transfer system. Finally, in Section 6, we present our conclusions.

## 2. Nonlinear two-port characteristics of bidirectional DC/DC converter

### 2.1 Bidirectional DC/DC converter as TVT

The bidirectional DC/DC converter is the basic power electronic circuit shown in Fig. 2.

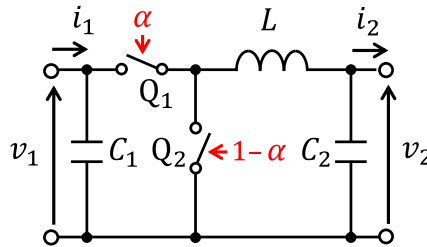


Fig. 2. Bidirectional DC/DC converter.

Switches  $Q_1$  and  $Q_2$  operate in a complementary manner. We drive switches by pulse-width modulation (PWM) with duty ratio  $\alpha$ . The duty ratio can be a time variable within the range  $0 \leq \alpha \leq 1$ . Ignoring the dynamics of  $C_1$ ,  $C_2$ , and  $L$ , the two-port characteristics are expressed as

$$\begin{bmatrix} v_1(k) \\ i_1(k) \end{bmatrix} = \begin{bmatrix} 1/\alpha(k) & 0 \\ 0 & \alpha(k) \end{bmatrix} \begin{bmatrix} v_2(k) \\ i_2(k) \end{bmatrix}. \quad (1)$$

Equation (1) is a TVT with a transformation ratio of  $\alpha(k)$ , where  $k$  is discrete time. The TVT is a lossless two-port circuit element; therefore, the port-to-port power relationship is  $v_1 i_1 = v_2 i_2$  [1, 5].

### 2.2 Nonlinear two-port characteristics

The bidirectional DC/DC converter was controlled using feedback. The control of the two-port characteristics is realized by feedback on the secondary-side operating points  $i_2$  and  $v_2$  to the duty ratio  $\alpha$ . The two-port characteristics generated by the feedback are formulated as follows:

$$\begin{bmatrix} v_1 \\ i_1 \end{bmatrix} = \begin{bmatrix} 1/\alpha(i_2, v_2) & 0 \\ 0 & \alpha(i_2, v_2) \end{bmatrix} \begin{bmatrix} v_2 \\ i_2 \end{bmatrix}. \quad (2)$$

The feedback of general DC/DC converters is provided to  $\alpha$  to maintain  $v_2$  or  $i_2$  constant. In this case, bidirectional DC/DC converters were used as the one-port circuits. It uses only the local conversion characteristics of the two-port circuits. However, the bidirectional DC/DC converter is a nonlinear two-port circuits that maps  $i_1$ - $v_1$  to  $i_2$ - $v_2$  characteristics. Therefore, we determine the target  $i_2$ - $v_2$  characteristics and provide feedback such that  $(i_2, v_2)$  are equilibria on the target characteristics.

### 2.3 Two operating points for single output

Assume that the power supply represented by Thevenin equivalent circuit connects to the primary-side of a bidirectional DC/DC converter, as shown in Fig. 1(a). Thevenin equivalent circuit is a typical power supply circuit, and the  $i_1$ - $v_1$  characteristics are expressed as

$$v_1 = e_1 - r_1 i_1. \quad (3)$$

In Eq. (3),  $r_1$  is the internal resistance and  $e_1$  is the internal electromotive force of the power supply. Substituting  $i_1$ - $v_1$  characteristics in Eq. (3) into Eq. (2) and eliminating  $i_1$ , the relationship between  $v_2$  and  $i_2$  is

$$v_2 = \alpha(i_2, v_2)e_1 - \alpha(i_2, v_2)^2 r_1 i_2. \quad (4)$$

Solving Eq. (4) for  $\alpha$ , we obtain the relationship between the secondary-side operating points  $(i_2, v_2)$  and the duty ratio  $\alpha$  as follows:

$$\alpha_{\pm}(i_2, v_2) = \frac{e_1 \pm \sqrt{e_1^2 - 4r_1 i_2 v_2}}{2r_1 i_2}. \quad (5)$$

A graphical representation of Eq. (5) in  $(i_2, v_2, \alpha)$  space is shown in Fig. 3.

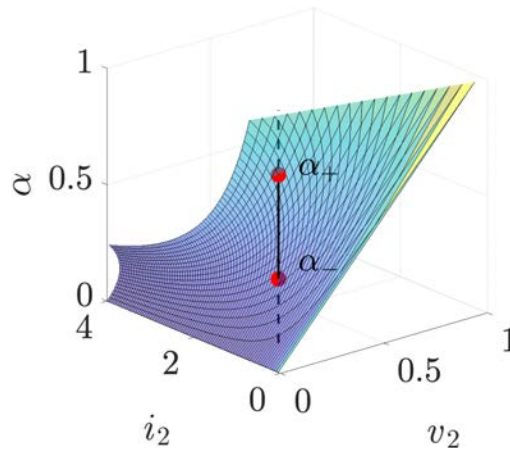


**Fig. 3.** Two operating points  $\alpha_+$ ,  $\alpha_-$  for single  $(i_2, v_2)$ .

As shown in Fig. 3, there are two duty ratios  $\alpha_+$  and  $\alpha_-$ ; therefore,  $(i_2, v_2)$  and  $\alpha$  are not uniquely determined because there are two combinations of  $(i_1, v_1)$  that satisfy the power relationship  $i_1 v_1 = i_2 v_2$  when  $v_2 i_2 < e_1^2 / 4r_1$ .

## 3. Elimination of untargeted equilibrium

### 3.1 Simple feedback based on target characteristics

We introduce simple feedback to realize the secondary-side characteristics. We realized the following secondary-side characteristics:

$$v_2 = e_2 - r_2 i_2. \quad (6)$$

A function that takes zero at  $(i_2, v_2)$  on the secondary-side characteristics of Eq. (6), we have

$$f_{iv}(i_2, v_2) = e_2 - r_2 i_2 - v_2. \quad (7)$$

Simple feedback of the DC/DC converter based on Eq. (6) is represented by:

$$\alpha(k+1) = \alpha(k) + K f_{iv}(i_2(k), v_2(k)). \quad (8)$$

$(i_2, v_2)$  satisfies Eq. (6), in the equilibrium states of Eq. (8). From Eq. (5), there are two duty ratios corresponding to the same  $(i_2, v_2)$ ; therefore, this feedback has two equilibrium points  $\alpha_+(i_2, v_2)$  and  $\alpha_-(i_2, v_2)$ .

### 3.2 Feedback to realize a unique equilibrium

We propose realizing feedback with a unique equilibrium by eliminating the untargeted equilibrium. We used  $\Delta\alpha$  instead of Eq. (7). When we changed the operating points  $(i_2, v_2)$  to  $(\Delta i_2 + i_2, \Delta v_2 + v_2)$ , there were two different variations in the duty ratio  $\Delta\alpha$  that corresponded to  $\Delta i_2$  and  $\Delta v_2$ . Substitute  $\Delta i_2 + i_2$ ,  $\Delta v_2 + v_2$ ,  $\Delta\alpha + \alpha$  for  $i_2$ ,  $v_2$ ,  $\alpha$  in Eq. (4) and rearrange as

$$r_1(i_2 + \Delta i_2)\Delta\alpha^2 - \{e_1 - 2\alpha r_1(i_2 + \Delta i_2)\}\Delta\alpha + \alpha^2 r_1 \Delta i_2 + \Delta v_2 = 0. \quad (9)$$

Solving Eq. (9) for  $\Delta\alpha$ , we obtain  $\Delta\alpha_+$  and  $\Delta\alpha_-$  as

$$\Delta\alpha_{\pm} = \frac{e_1}{2r_1(i_2 + \Delta i_2)} - \alpha \pm \frac{\sqrt{[e_1 - 2\alpha r_1(i_2 + \Delta i_2)]^2 - 4r_1(\alpha^2 r_1 \Delta i_2 + \Delta v_2)(i_2 + \Delta i_2)}}{2r_1(i_2 + \Delta i_2)}. \quad (10)$$

By substituting Eq. (5) to  $\alpha$  in Eq. (10) and set  $\Delta i_2 = \Delta v_2 = 0$ , the values of  $\Delta\alpha_+$  and  $\Delta\alpha_-$  on  $\alpha_+$  and  $\alpha_-$  are evaluated, as shown in Table I.

**Table I.** Equilibrium state and two duty ratios in Eq. (10).

Eq. (10)	on $\alpha_+$	on $\alpha_-$
$\Delta\alpha_+$	$= 0$	$\neq 0$
$\Delta\alpha_-$	$\neq 0$	$= 0$

If we use  $\Delta\alpha_+$  for the feedback, the equilibrium is  $\alpha_+$ . Similarly, if we use  $\Delta\alpha_-$ , the equilibrium is  $\alpha_-$ . From the simple feedback concept, we use the following equations to obtain  $\Delta i_2$  and  $\Delta v_2$ .

$$\begin{cases} \Delta i_2 = K_i f_{iv}(i_2, v_2) \\ \Delta v_2 = K_v f_{iv}(i_2, v_2) \end{cases}. \quad (11)$$

$K_i$  and  $K_v$  are the gains of  $\Delta i_2$  and  $\Delta v_2$ . Let us now discuss the case of selecting  $\alpha_-$ . Substituting Eq. (10), and Eq. (11) for  $\alpha(k+1) = \alpha(k) + \Delta\alpha_-$ , the following is obtained.

$$\begin{aligned} \alpha(k+1) &= A(k) - \text{sgn}(A(k))\sqrt{(A(k) - \alpha(k))^2 - B(k)} \\ A(k) &= \frac{e_1}{2r_1\{(1 - K_i r_2)i_2(k) + K_i(e_2 - v_2(k))\}} \\ B(k) &= \frac{(\alpha(k)^2 r_1 K_i + K_v)(e_2 - v_2(k) - r_2 i_2(k))}{r_1\{(1 - K_i r_2)i_2(k) + K_i(e_2 - v_2(k))\}}. \end{aligned} \quad (12)$$

By using Eq. (12), we obtain feedback to realize unique mapping  $(i_2, v_2)$  to  $\alpha_-$ . However, with the exception of  $i_2 = 0$ . Furthermore, if  $\Delta i_2$  and  $\Delta v_2$  satisfy  $(\Delta i_2 + i_2)(\Delta v_2 + v_2) > e_1^2/4r_1$  in the feedback,  $\Delta\alpha$  becomes a complex number. This event occurs when the operating point of the primary-side corresponds to that of the secondary-side  $(\Delta i_2 + i_2)(\Delta v_2 + v_2)$ . Exception handling is required to avoid feedback failure owing to this event, which we discuss in Section 4.2.

## 4. Global stabilization of stand-alone converter

### 4.1 System with static load

The operating point of the secondary-side was determined by connecting a load to the bidirectional DC/DC converter. We connected the loads represented by Thevenin equivalent circuit. The circuit system when the load was connected is shown in Fig. 4.

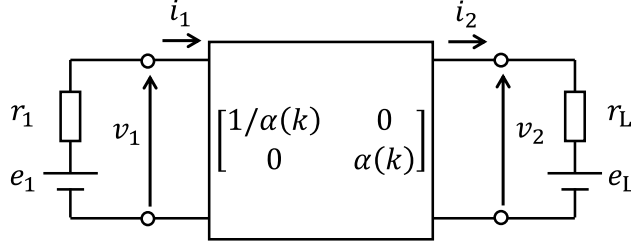


**Fig. 4.** Bidirectional DC/DC converter with load and power supply.

From Fig. 4,  $i_2$  and  $v_2$  at  $\alpha(k)$  appear as following equations.

$$i_2(\alpha(k)) = \frac{\alpha(k)e_1 - e_L}{r_1\alpha(k)^2 + r_L}. \quad (13)$$

$$v_2(\alpha(k)) = e_L + r_L \frac{\alpha(k)e_1 - e_L}{r_1\alpha(k)^2 + r_L}. \quad (14)$$

### 4.2 Global stabilization by setting gain

We define the return-map  $f$  as the mapping from  $\alpha(k)$  to  $\alpha(k+1)$ , as shown in

$$\alpha(k+1) = f(\alpha(k)), \quad \alpha(k) \in [0, 1]. \quad (15)$$

The return-map  $f$  is a nonlinear mapping representing the transients of duty ratio  $\alpha$ . The return-map of the simple feedback is obtained by substituting Eq. (13), (14) into Eq. (8). Similarly, the return-map of the proposed feedback is obtained by substituting Eq. (13), (14) into Eq. (12); When considering global stability using maps, it is important to determine how the operating points converge to equilibrium. We assume  $f$  has a stable equilibrium point  $\alpha^*$ . We define the contraction ratio of the map centered at  $\alpha^*$  as follows:

$$\mu(\alpha) = \frac{|\alpha^* - f(\alpha)|}{|\alpha^* - \alpha|}. \quad (16)$$

If  $\mu(\alpha) < 1$ ,  $\alpha(k) \in [0, 1]$ , the application of  $f$  to  $\alpha(k)$  converges the operating point to  $\alpha^*$ .

The proposed feedback return-map had only one equilibrium point. Therefore, global stability is guaranteed by setting gains  $K_i$  and  $K_v$  such that  $\mu(\alpha) < 1$ ,  $\alpha(k) \in [0, 1]$  holds. When  $\mu = 0$  in Eq. (16), the return-map corresponds to the feedback that reaches equilibrium in one discrete step as follows:

$$\alpha^* = f(\alpha), \quad \alpha(k) \in [0, 1]. \quad (17)$$

The gain satisfying  $\mu = 0$  was calculated from the proposed feedback return-map as follows:

$$K_i = K_v = \frac{(e_L r_1 \alpha_- + e_1 r_L) \alpha_-}{(e_2 r_L + e_L r_2)(1 + r_1 \alpha_-^2)}. \quad (18)$$

Thus, we achieve global stability by setting the gain to Eq. (18). In addition, we can expect that the gains  $K_i$  and  $K_v$  are close to the values in Eq. (18) satisfies  $0 < \mu < 1$ . However, if the gain does not satisfy Eq. (18), the calculated duty ratio occasionally becomes a complex number, as described in Section 3.2. If the duty ratio becomes a complex number, feedback failure is avoided by using the gain in Eq. (18).

### 4.3 Example of return-map

Return-maps of the simple feedback and the proposed feedback are shown in Fig. 5(a) and Fig. 6(a), respectively. In both return-maps, the circuit parameters are  $e_1 = 100$  V,  $r_1 = 20$   $\Omega$ ,  $e_2 = 50$  V,  $r_2 = 7$   $\Omega$ ,  $e_L = 0$  V,  $r_L = 3$   $\Omega$ , and the gain of each map is shown in the figures. The primary-side parameters  $e_1 = 100$  V and  $r_1 = 20$   $\Omega$  are set to allow for continuous short-circuit operation to verify the global stability at  $\alpha(k) \in [0, 1]$  in the experiment. Moreover, we calculated the contraction ratio  $\mu(\alpha)$  of the map centered at  $\alpha_-$  from the return-maps in Fig. 5(a) and Fig. 6(a) is shown in Fig. 5(b) and Fig. 6(b).

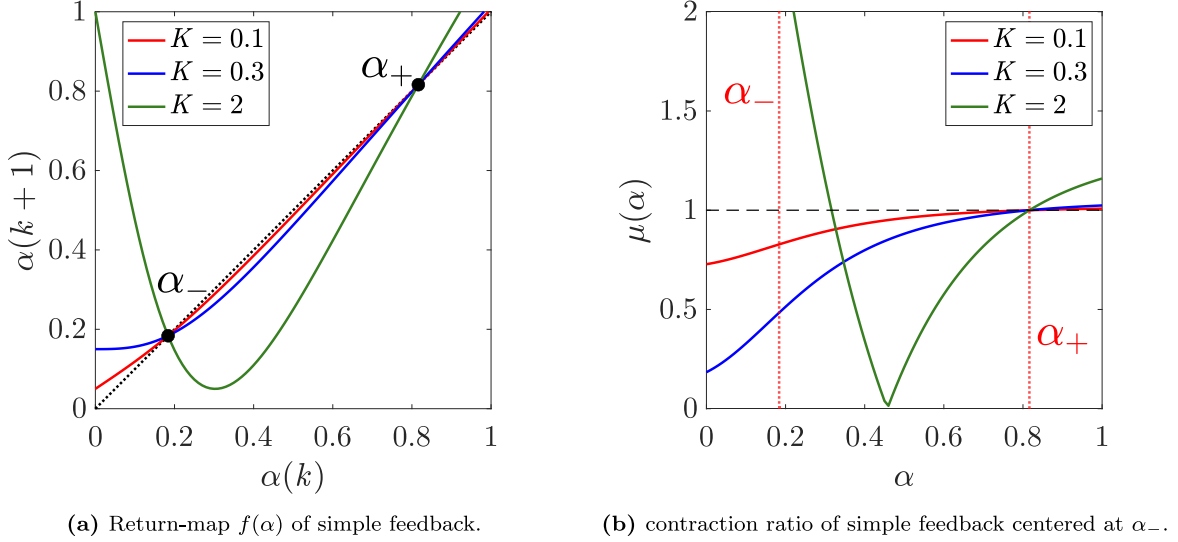


**Fig. 5.** Simulation result of simple feedback.

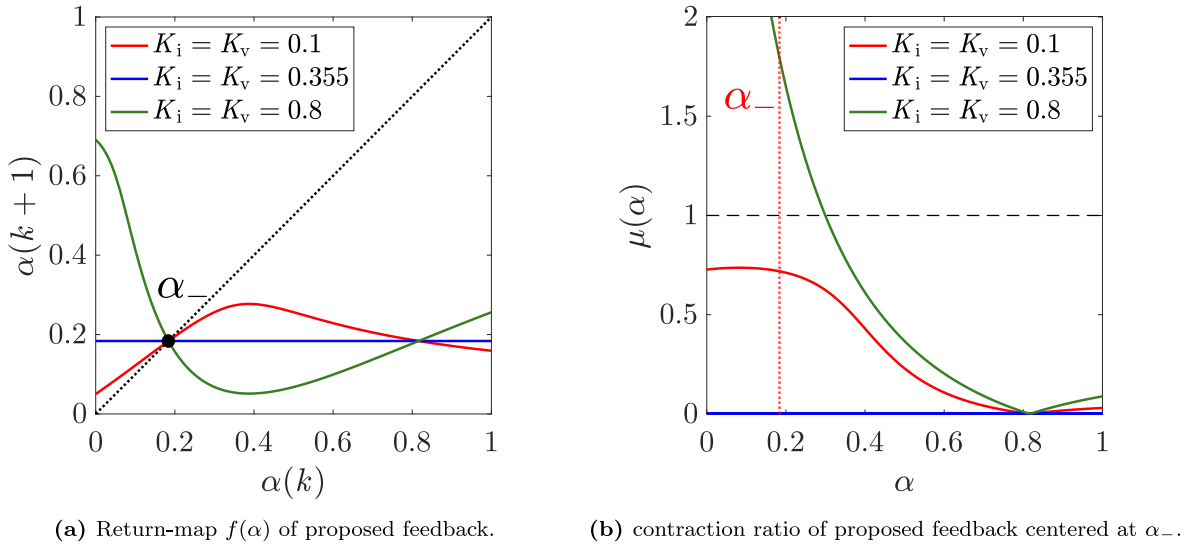


**Fig. 6.** Simulation result of proposed feedback.

From Fig. 5(a), simple feedback has two equilibrium points  $\alpha_-$  and  $\alpha_+$ ; therefore, simple feedback does not have a unique equilibrium. In Fig. 5(b), the return-map of the simple feedback takes  $\mu > 1$  in the regions  $\alpha > \alpha_+$  regardless of the gain. Although simple feedback cannot achieve global stability at any gain, it realizes partial stability in the region of  $\alpha < \alpha_+$  when  $K = 0.1$  and  $K = 0.3$ , as shown in Fig. 5(b). However, the proposed feedback has only one equilibrium point,  $\alpha_-$  in Fig. 6(a). When the gain is set to  $K_i = K_v = 0.355$  calculated from Eq. (18), we can observe that  $\mu(\alpha) = 0$ ,  $\alpha(k) \in [0, 1]$  in Fig. 6(b) and global stability is guaranteed. As we change the gain from  $K_i = K_v = 0.355$ , the contraction ratio becomes greater than zero. However, global stability is achieved within the range

that satisfies  $\mu < 1$ , such as  $K_i = K_v = 0.1$ . If we set the gain beyond this range, the region of  $\mu > 1$  occurs, as in  $K_i = K_v = 0.8$ , and global stability is lost.

#### 4.4 Experimental demonstration

We verified the stability of the simple feedback and the proposed feedback using a bidirectional DC/DC converter. Figure 7 shows the SiC bidirectional converter module used in the experiments. The specifications of this bidirectional converter module are shown in Appendix A. We set the circuit and target parameters to the same values as the return-map conditions in Section 4.3. The gains for each feedback were set to  $K = 0.3$  and  $K_i = K_v = 0.355$ . Feedback control was implemented on the microcontroller and controlled for 33 ms cycles. Because this control period is larger than the time constant of the bidirectional DC/DC converter, the bidirectional DC/DC converter functions as the TVT.



**Fig. 7.** SiC bidirectional converter module.

Global stability was verified by setting the initial values of  $\alpha(k)$  to 0.1, 0.5, and 0.9. The transient responses of the simple feedback acquired from the experiments are shown in Fig. 8 and the transients of the proposed feedback are shown in Fig. 9. We applied the feedback 100 ms from the start of the measurement.

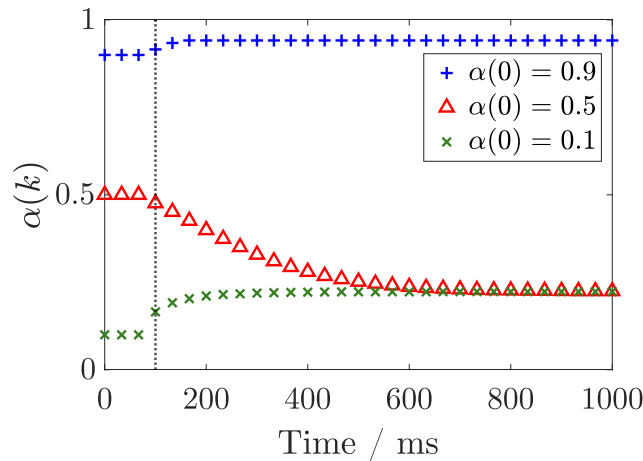


**Fig. 8.** Transient waveform of  $\alpha(k)$  when we apply the simple feedback. ( $K = 0.3$ ).

From Fig. 8, simple feedback exhibits a divergent transient response of  $\alpha(0) = 0.9$ . Therefore, it does not exhibit global stability. However, as shown in Fig. 9, in the proposed feedback, all operating points converge to an equilibrium point and achieve global stability. Ideally, the transient response



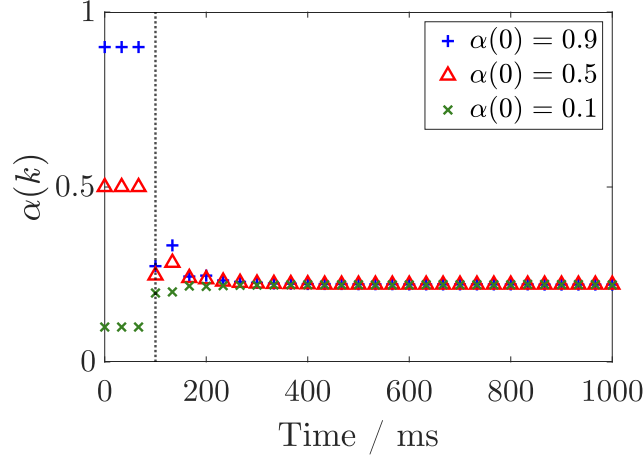


**Fig. 9.** Transient waveform of  $\alpha(k)$  when we apply the proposed feedback. ( $K_i = K_v = 0.355$ ).

converges in a discrete step. But in Fig. 9, several steps were required for convergence. Possible causes include the loss of the bidirectional DC/DC converter and the error of the current transducer.

## 5. Stabilize peer-to-peer energy transfer system with two converters

### 5.1 Peer-to-peer energy transfer system

A peer-to-peer energy transfer system [20] is a power system that provides decoupling from a common bus. Peer-to-peer energy transfer achieves decoupling by synchronous control between bidirectional converters connected to the bus. This section deals with the global stabilization of simple peer-to-peer energy transfer systems for DC power transmission. As a simple case of without a voltage source, a peer-to-peer energy transfer system with two bidirectional DC/DC converters is shown in Fig. 10.

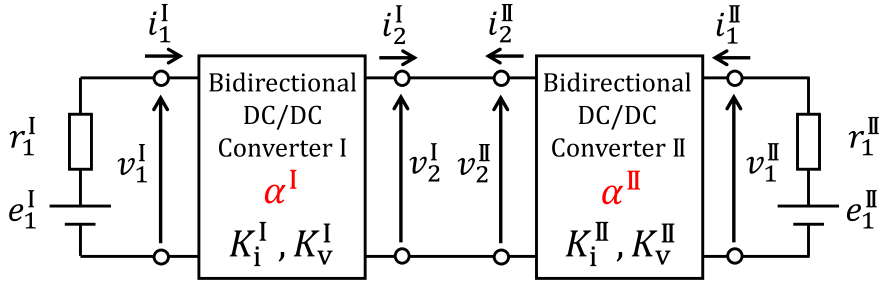


**Fig. 10.** Peer-to-peer energy transfer system with two converters.

The two bidirectional DC/DC converters can communicate via a wireless communication network, and their duty ratios are changed synchronously. The timing synchronization protocol is shown in Appendix B. In Fig. 10,  $i_2^I(k) = -i_2^{II}(k)$  and  $v_2^I(k) = v_2^{II}(k)$  hold between the two bidirectional DC/DC converters. Therefore, the target operating points  $(i_2^{I*}, v_2^{I*})$  and  $(i_2^{II*}, v_2^{II*})$  should be satisfied.

### 5.2 Feedback method targeting the operating point

The peer-to-peer energy transfer system can synchronize the target operating points of the supply and load through wireless communication between converters. Therefore, we propose feedback that targets the operating point instead of the target secondary-side characteristics described in Section 4.

In the standalone converter, we provide  $\Delta i_2$  and  $\Delta v_2$  using Eq. (11). Now, we propose  $\Delta i_2$  and  $\Delta v_2$  for peer-to-peer energy transfer as follows:

$$\begin{cases} \Delta i_2^\dagger = K_i^\dagger (i_2^{\dagger*} - i_2^\dagger) \\ \Delta v_2^\dagger = K_v^\dagger (v_2^{\dagger*} - v_2^\dagger) \end{cases} \quad (\dagger = \text{I, II}). \quad (19)$$

We substitute Eq. (10), and Eq. (19) for  $\alpha(k+1) = \alpha(k) + \Delta\alpha_-$ , we obtain

$$\begin{aligned}
\alpha^\dagger(k+1) &= A^\dagger(k) - \text{sgn}(A^\dagger(k))\sqrt{(A^\dagger(k) - \alpha^\dagger(k))^2 - B^\dagger(k)} \\
A^\dagger(k) &= \frac{e_1^\dagger}{2r_1^\dagger\{K_1^\dagger i_2^{\dagger*} + (1 - K_1^\dagger)i_2^\dagger(k)\}} \\
B^\dagger(k) &= \frac{\alpha^\dagger(k)^2 r_1^\dagger K_1^\dagger (i_2^{\dagger*} - i_2^\dagger(k)) + K_v^\dagger (v_2^{\dagger*} - v_2^\dagger(k))}{r_1^\dagger\{K_1^\dagger i_2^{\dagger*} + (1 - K_1^\dagger)i_2^\dagger(k)\}}
\end{aligned} \tag{20}$$

Because  $\Delta\alpha_-$  only has equilibrium  $\alpha_-$  from Table I,  $\alpha_+(i_2^{\dagger*}, v_2^{\dagger*})$  is not an equilibrium point in Eq. (20). When this feedback is applied, the only equilibrium point that corresponds to  $(i_2^{\dagger*}, v_2^{\dagger*})$  is  $\alpha_-(i_2^{\dagger*}, v_2^{\dagger*})$ . Thus, we achieve a unique equilibrium point in the individual converters.

### 5.3 Global stabilization of two converters coupled by a bus

The previous section described how to achieve unique equilibrium points in individual converters in a peer-to-peer energy transfer system. We apply the feedback in Eq. (20) for the individual converters in the system in Fig. 10 and set the target to satisfy  $i_2^{I*} = -i_2^{II*}$  and  $v_2^{I*} = v_2^{II*}$  results in a unique equilibrium point for the entire system. Then, we set the gain satisfying  $K_1^I = K_1^{II}$  and  $K_v^I = K_v^{II}$  to match the duty ratio transients of the supply and load. The same concept as in Section 4.2 can be used to guarantee global stability even when there are two converters in the system.

We define the duty ratio vector as  $\alpha(k) = [\alpha^I(k), \alpha^{II}(k)]^T$ , and thus, the feedback to the two converters  $\mathbf{f} : \alpha(k) \rightarrow \alpha(k+1)$  is formulated as follows:

$$\alpha(k+1) = \mathbf{f}(\alpha(k)) \tag{21}$$

where we assume that  $\mathbf{f}$  has only one equilibrium point  $\alpha^*$  and we define the contraction ratio of the map centered at  $\alpha^*$  as follows:

$$\mu(\alpha) = \frac{|\alpha^* - \mathbf{f}(\alpha)|}{|\alpha^* - \alpha|}. \tag{22}$$

where  $\mu(\alpha) < 1$ ,  $\alpha(k) \in [0, 1]^2$ , and then repeatedly applying  $\mathbf{f}$  to  $\alpha(k)$  converges the operating points to  $\alpha^*$ .  $|\cdot|$  is the distance at  $\mathbb{R}^2$ , and  $[a, b]^2$  is the direct product of  $[a, b]$ . As discussed in Section 4.2, this nonlinear mapping converges the operating points to the equilibrium point in one discrete step when  $\mu = 0$  is satisfied as follows:

$$\alpha^* = \mathbf{f}(\alpha), \quad \alpha(k) \in [0, 1]^2. \tag{23}$$

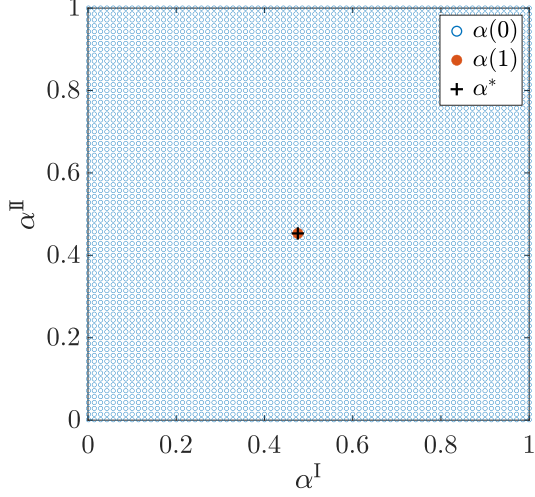
In this system,  $\mu = 0$  corresponds to the case where the gains are set to  $K_1^\dagger = K_v^\dagger = 1$  ( $\dagger = I, II$ ) and we achieve global stability.  $\Delta i_2^\dagger = i_2^{\dagger*} - i_2^\dagger$  and  $\Delta v_2^\dagger = v_2^{\dagger*} - v_2^\dagger$  holds when the gains are set. In addition, global stability is achieved when  $K_1^\dagger = K_v^\dagger \neq 1$  using gains in the region satisfying  $0 < \mu < 1$ . In addition, there are cases in which Eq. (20) is complex in  $K_1^\dagger = K_v^\dagger \neq 1$ , in which case we avoid it by setting  $K_1^\dagger = K_v^\dagger = 1$ .

Nonlinear mapping is computed and illustrated to visually confirm global stability. We show a map with  $K_1^\dagger = K_v^\dagger = 1$  in Fig. 11(a) and the map with  $K_1^\dagger = K_v^\dagger = 0.5$  in Fig. 12(a). The contraction ratios calculated from the respective maps are shown in Fig. 11(b) and Fig. 12(b).

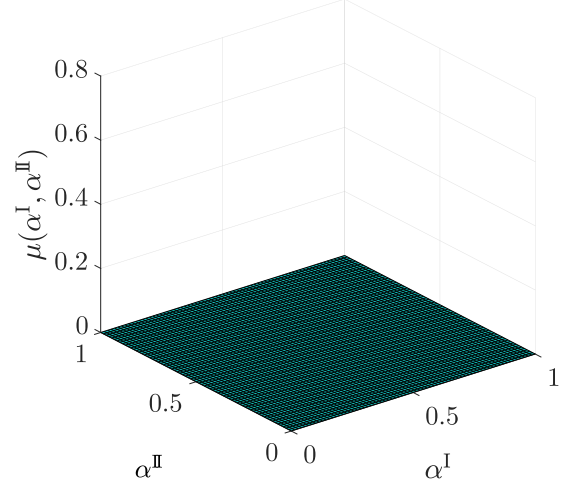
In Fig. 11(a), all the operating points converge to the equilibrium point  $\alpha^*$  in one step. The contraction ratio of this map was  $0 = \mu(\alpha)$  at  $\alpha(0) \in [0, 1]^2$ , as shown in Fig. 11(b), which achieved global stability. The green markers shown in Fig. 12(a) represent the region in which the results of Eq. (20) take a complex number when  $K_1^\dagger = K_v^\dagger = 0.5$  and the map is calculated with the gain set to  $K_1^\dagger = K_v^\dagger = 1$  only in this region. As shown in Fig. 12(b), the region where the contraction ratio is zero by this exception. For the other region, the contraction ratio is within the range  $0 < \mu(\alpha) < 1$ ; thus, global stability is achieved in  $K_n^i = K_n^v = 0.5$  using exception handling.

### 5.4 Experimental demonstration

We demonstrate a peer-to-peer energy transfer system using two bidirectional DC/DC converters. Two SiC bidirectional converter modules were used, as shown in Fig. 7. The system architecture is

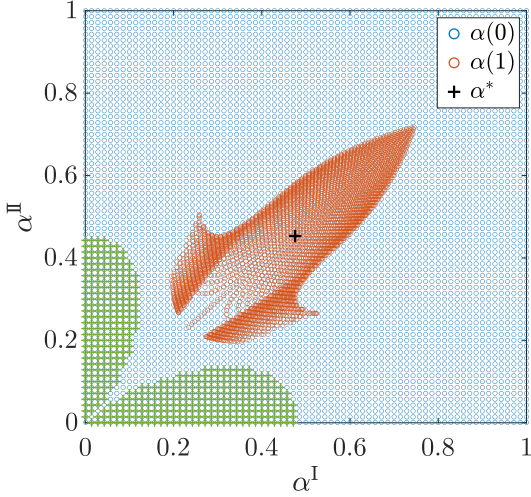


(a) Map of feedback  $f : \alpha(0) \rightarrow \alpha(1)$ .

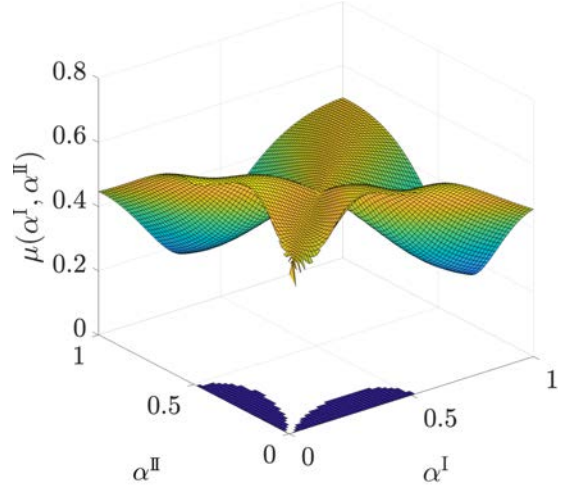


(b) Contraction ratio  $\mu(\alpha)$ .

**Fig. 11.** Simulation result with  $K_i^\dagger = K_v^\dagger = 1$  ( $\dagger = \text{I, II}$ ).



(a) Map of feedback  $f : \alpha(0) \rightarrow \alpha(1)$ . The green markers shown represent the region in which the results of Eq. (20) take a complex number.

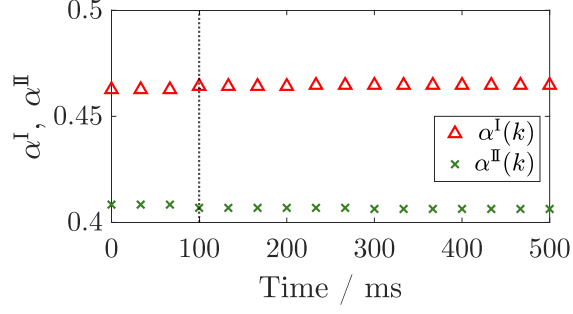


(b) Contraction ratio  $\mu(\alpha)$ . The dark blue plots shown the region set to  $K_i^\dagger = K_v^\dagger = 1$  by exception handling.

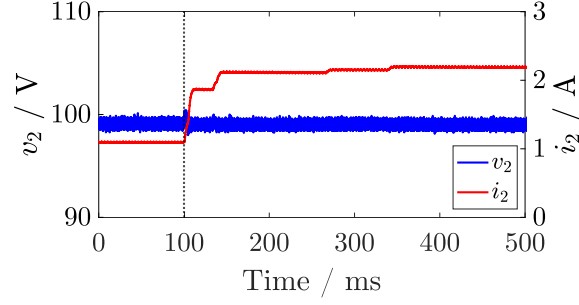
**Fig. 12.** Simulation result with  $K_i^\dagger = K_v^\dagger = 0.5$  ( $\dagger = \text{I, II}$ ).

the same as that in Fig. 10, we used lithium-ion batteries with the characteristics of  $e_1^{\text{I}} = e_1^{\text{II}} = 215 \text{ V}$  and  $r_1^{\text{I}} = r_1^{\text{II}} = 5 \text{ } \Omega$ . The gains were set to  $K_i^\dagger = K_v^\dagger = 1$  ( $\dagger = \text{I, II}$ ). We set the initial values of the secondary-side operating points  $(i_2^{\text{I}}, v_2^{\text{I}})$  at  $(1 \text{ A}, 100 \text{ V})$  and  $(3 \text{ A}, 100 \text{ V})$ . We measured the transients and changed the targets 100 ms from the start of the measurement. Figure 13(a) shows the experimental results of peer-to-peer energy transmission in  $(i_2^{\text{I}}, v_2^{\text{I}}) = (1 \text{ A}, 100 \text{ V})$  and Fig. 14(a) shows the experimental results in  $(i_2^{\text{I}}, v_2^{\text{I}}) = (3 \text{ A}, 100 \text{ V})$ .

In Figs. 13 and 14, the duty ratios and operating points move to near steady states at 100 ms and converge after several transition steps. The duty ratios converged to the same equilibrium point, and the effect of the untargeted equilibrium points was not apparent. Although the bus voltage fluctuated slightly during the transient process, the width of the fluctuation was the same as that caused by switching. However, steady-state deviation occurs at the equilibrium point. One possible cause of the steady-state deviation that can be confirmed by the experimental results is the error in the current transducer.

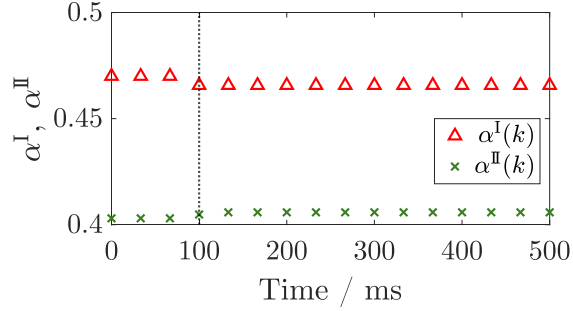


(a) Transient waveform of  $\alpha(k)$ .

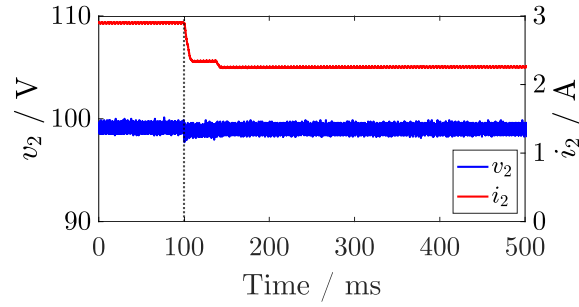


(b) Transient waveform of  $i_2^I$  and  $v_2^I$ .

**Fig. 13.** Experimental result of peer-to-peer energy transfer with  $i_2^I$  changed from 1 A to 2 A.



(a) Transient waveform of  $\alpha(k)$ .



(b) Transient waveform of  $i_2^I$  and  $v_2^I$ .

**Fig. 14.** Experimental result of peer-to-peer energy transfer with  $i_2^I$  changed from 3 A to 2 A.

## 6. Conclusions

We modeled the bidirectional DC/DC converter as a TVT, and we showed that its two-port characteristics are formulated as nonlinear two-port characteristics by applying feedback to the TVT. This nonlinear two-port characteristic is due to the nonlinearity of the power relationship between ports. The power relationship results in two primary-side operating points corresponding to one secondary-side operating point. When simple feedback targeting secondary-side characteristics is applied to the bidirectional DC/DC converter, global stability is not achieved owing to the untargeted equilibrium

point. Therefore, we propose a feedback method that eliminates untargeted equilibrium points using a power relationship. We achieve global stabilization in our proposed feedback system by setting the gain to guarantee convergence for the target equilibrium point. We applied simple feedback and the proposed method to the stand-alone converter, and we confirmed the global stability of the proposed method experimentally. As an application of the proposed method, we proposed the global stabilization of the peer-to-peer energy transfer system and confirmed its validity through an experimental demonstration.

Our results provide a method for creating a unique equilibrium point and stabilizing the equilibrium in circuit systems with power nonlinearities. In this article, we introduce the stabilization of a bidirectional DC/DC converter connected to a simple supply represented by a Thevenin equivalent circuit. Because the multiple equilibrium points in the converter are due to power relationships, the proposed concept can be applied for the global stabilization of converter systems that include supplies with complicated  $i$ - $v$  characteristics.

## Acknowledgments

This work was supported by the Grants-in-Aid for Scientific Research under Grant 22K04103.

## Appendix

### A. Specifications of converter module

The overview of converter module is shown in Fig A-1, and the circuit parameters of converter are listed in Table A-I. And, Table A-II lists the rated specifications of the converter modules.

The two switches are ROHM SCT2080KE and the PWM frequency is 30 kHz. A microcontroller is used to control the converter, and the secondary side voltage  $v_2$  and current  $i_2$  are sensed by the 10-bit A/D converter. The ZigBee module is used for wireless communication in the peer-to-peer energy transfer experiment described in Section 5.

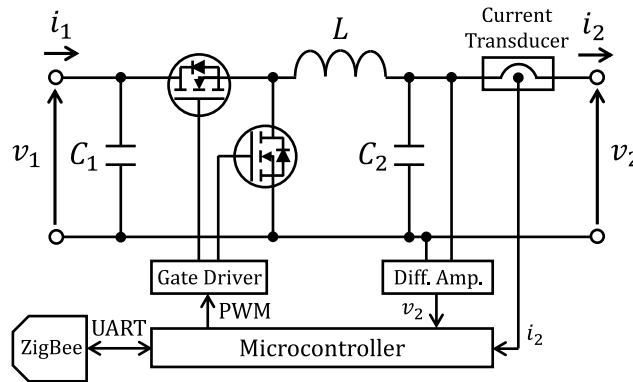


**Fig. A-1.** Overview of the bidirectional converter module.

**Table A-I.** Circuit parameters of the converter module.

Components	Value
$C_1$	471 $\mu\text{F}$
$C_2$	9.4 $\mu\text{F}$
$L$	1.4 mF

**Table A-II.** Rated specifications.

Parameters	Value
$v_1$	250 V
$i_1$	6 A
$v_2$	150 V
$i_2$	10 A

## B. Protocol for timing synchronization on DC peer-to-peer energy transfer

The peer-to-peer energy transfer concept requires synchronization of the timing of output change between two converter modules. The protocol for synchronizing and compensating the communication delay in an AC peer-to-peer energy transfer system is described in [20]. The basic protocol for synchronization between two modules in a DC system is the same as that in an AC system, with only the start timing of the output change being different. The AC system can use the zero crossing of the secondary-side voltage to synchronize the output change. In contrast, the secondary-side voltage of the DC system is constant. Therefore, the protocol shown in Fig. B-1 was used for this DC peer-to-peer energy transfer.

The flow of this protocol is as follows:

- (I) The microcontroller in Module 1 transmit a synchronization command via ZigBee to the UART. When the UART transfer is complete, Module 1 sends a synchronization command to Module 2 via ZigBee.
- (II) When Module 2 receives the first byte of the synchronization command from Module 1 via ZigBee, it immediately sends back an ACK to Module 1 via ZigBee.
- (III) Module 1 receives an ACK from Module 2 and records  $t_2 - t_1$  as  $T_{ACK}$ .
- (IV) Module 2 sends  $T_{R-int}$  to Module 1. This  $T_{R-int}$  is the internal delay for processing in Module 2, and this value is maintained by Module 2.
- (V) Module 1 calculates its wait time  $T_{wait}$  using the received  $T_{R-int}$ . This  $T_{wait}$  is estimated by  $T_{wait} = T_{R-int} + T_{ACK}/2$ .
- (VI) Module 1 send a start command to Module 2 and waits for  $T_{wait}$ . When the wait is complete, Module 1 starts to change outputs. Module 2 also initiates the output change when it receives the start command.
- (VII) Module 2 receives the start command and starts to change the output.

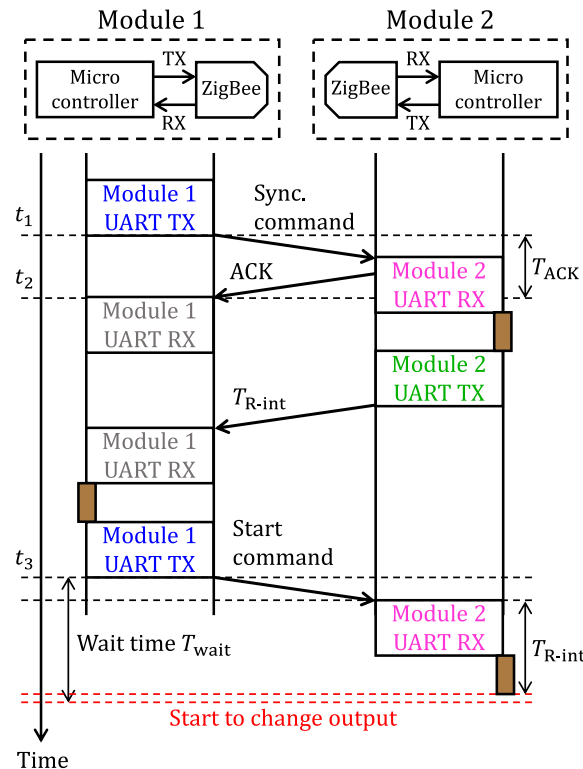


**Fig. B-1.** Overview of the synchronization protocol.

In this protocol, if control timing deviations occur when the delay time changes from the measured delay. However, this delay variation is less than 1 ms in our experimental system, which is smaller than the feedback update period (33 ms) and the time constant of the converter. Therefore, the effect of delay variation is small in this system.

## References

- [1] S. Singer and R.W. Erickson, "Canonical modeling of power processing circuits based on the POPI concept," *IEEE Transactions on Power Electronics*, vol. 7, no. 1, pp. 37–43, January 1992. DOI: 10.1109/63.124575
- [2] R.D. Middlebrook and S. Cuk, "A general unified approach to modelling switching-converter power stages," *1976 IEEE Power Electronics Specialists Conference*, pp. 18–34, June 1976. DOI: 10.1109/PESC.1976.7072895
- [3] D. Shmilovitz, "Loss-free complex impedance network elements," *IEEE Transactions on Circuits and Systems I*, vol. 253, no. 3, pp. 704–711, March 2006. DOI: 10.1109/TCSI.2005.859573
- [4] B.D. Anderson, D.A. Spaulding, and R.W. Newcomb, "The time-variable transformer," *Proceedings of the IEEE*, vol. 53, no. 6, pp. 634–635, June 1965. DOI: 10.1109/PROC.1965.3948
- [5] S. Singer, S. Efrati, Me. Alon, and D. Shmilovitz, "Maximum electrical power extraction from sources by Load matching," *Energies*, vol. 20, no. 8025, December 2021. DOI: 10.3390/en14238025
- [6] S. Singer, "Loss-free gyrator realization," *IEEE Transactions on Circuits and Systems*, vol. 35, no. 1, pp. 26–34, January 1988. DOI: 10.1109/31.1697
- [7] A.P.N. Tahim, D.J. Pagano, and E. Ponce, "Nonlinear control of dc-dc bidirectional converters in stand-alone dc Microgrids," *IEEE 51st IEEE Conference on Decision and Control*, pp. 3068–3073, December 2012. DOI: 10.1109/CDC.2012.6426298
- [8] A.P.N. Tahim, D.J. Pagano, M.L. Heldwein, and E. Ponce, "Control of interconnected power electronic converters in dc distribution systems," *XI Brazilian Power Electronics Conference*, pp. 269–274, September 2011. DOI: 10.1109/COBEP.2011.6085269
- [9] R. Cristiano, D.J. Pagano, L. Benadero, and E. Ponce, "Bifurcation Analysis of a DC-DC Bidirectional Power Converter Operating with Constant Power Loads," *International Journal of Bifurcation and Chaos*, vol. 26, no. 4, pp. 1630010:1–1630010:22, April 2016. DOI: 10.1142/S021812741630010X
- [10] H. Bae, J. Lee, S. Park, and B.H. Cho, "Large-signal stability analysis of solar array power system," *IEEE Transactions on Aerospace and Electronic Systems*, vol. 44, no. 2, pp. 538–547, April 2008. DOI: 10.1109/TAES.2008.4560205
- [11] J.H. Lee, H.S. Bae, and B.H. Cho, "Resistive control for a photovoltaic battery charging system using a microcontroller," *IEEE Transactions on Industrial Electronics*, vol. 55, no. 7, pp. 2767–2775, July 2008. DOI: 10.1109/TAES.2008.4560205
- [12] L. Guo, L. Xu, K. Sun, and Y. Li, "Stability analysis of stand-alone photovoltaic system considering controller time delay," *IEEE 4th Conference on Energy Internet and Energy System Integration*, pp. 57–62, November 2020. DOI: 10.1109/EI250167.2020.9347340
- [13] E. Lenz, D. Pagano, and A.P.N. Tahim, "Codimension-two bifurcation analysis in DC microgrids under droop control," *International Journal of Bifurcation and Chaos*, vol. 26, no. 2, pp. 1650028:1–1650028:22, February 2016. DOI: 10.1142/S0218127416500280
- [14] A. Isidori *Nonlinear Control Systems Third Edition*, Springer, London, 1995.
- [15] Z. Madni, K. Guesmi, and A. Benalia, "Backstepping global and structural stabilization of direct current/direct current boost converter," *International Journal of Circuit Theory and Applications*, vol. 50, no. 13, pp. 1604–1619, February 2022. DOI: 10.1002/cta.3237
- [16] W. Zhou and X. Ye, "Adaptive control of parallel DC-DC buck converters with uncertain parameters," *12th International Conference on Control Automation Robotics & Vision*, pp. 737–740, December 2012. DOI: 10.1109/ICARCV.2012.6485249
- [17] P. Magne, B. Nahid-Mobarekeh, and S. Pierfederici, "General Active Global Stabilization of Multiloading DC-Power Networks," *IEEE Transactions on Power Electronics*, vol. 27, no. 4,

- pp. 1788–1798, September 2011. DOI: 10.1109/TPEL.2011.2168426
- [18] R. Ortega, A. Loría, P.J. Nicklasson, and H. Sira-Ramírez, *Passivity-Based Control of Euler-Lagrange Systems*, Springer, London, 1998.
  - [19] A. Kwasinski and P.T. Krein, “Passivity-Based Control of Buck Converters with Constant-Power Loads,” *2007 IEEE Power Electronics Specialists Conference*, vol. 50, no. 13, pp. 259–265, June 2007. DOI: 10.1109/PESC.2007.4341998
  - [20] D. Kiss, T. Hisakado, T. Matsushima, and O. Wada, “Peer-to-peer energy transfer by Power Gytrators based on time-variable-transformer concept,” *IEEE Transactions on Power Electronics*, vol. 34, no. 8, pp. 8230–8240, August 2019. DOI: 10.1109/TPEL.2018.2882129